Tissue Engineering and Regenerative Medicine

Aortic valve cell seeding into decellularized animal pericardium by perfusion-assisted bioreactor

Journal:	*Journal of Tissue Engineering and Regenerative Medicine*
Manuscript ID	TERM-17-0407.R1
Wiley - Manuscript type:	Research Article
Date Submitted by the Author:	08-Feb-2018
Complete List of Authors:	Amadeo, Francesco; Centro cardiologico Monzino, IRCCS, Laboratorio di Ingegneria Tissutale Cardiovascolare Boschetti, Federica; Politecnico di Milano, LaBs Polvani, Gianluca; Università di Milano, Dipartimento di Scienze Cliniche e di Comunità Banfi, Cristina; Centro Cardiologico Monzino, Unità di Proteomica Pesce, Maurizio; Centro cardiologico Monzino, IRCCS, Unità di Ingegneria Tissutale Cardiovascolare Santoro, Rosaria; Centro cardiologico Monzino, IRCCS, Unità di Ingegneria Tissutale Cardiovascolare
Keywords:	Pericardium, decellularization, xenoantigen, valve interstitial cell, tissue engineered heart valve, bioreactor

Aortic valve cell seeding into decellularized animal pericardium by perfusion-assisted bioreactor

Francesco Amadeo[1], Federica Boschetti[2], Gianluca Polvani[3], Cristina Banfi[4], Maurizio Pesce[1, *, §], Rosaria Santoro[1, §]

1. Unità di Ingegneria Tissutale Cardiovascolare, Centro Cardiologico Monzino, IRCCS; Milan, Italy
2. LaBs, Politecnico di Milano; Milan, Italy
3. Dipartimento di Scienze Cliniche e di Comunità; Università di Milano
4. Unità di Proteomica, Centro Cardiologico Monzino IRCCS; Milan, Italy

*Corresponding Author: Maurizio Pesce, Centro Cardiologico Monzino, IRCCS; Via C. Parea, 4; I-20138, Milan, Italy

§ These Authors contributed equally to this study

Running head: Recellularization of animal pericardium for valve engineering

Keywords: Pericardium; decellularization; xenoantigen; valve interstitial cell; tissue engineered heart valve; bioreactor

ABSTRACT

Animal-derived pericardium is the elective tissue employed in manufacturing heart valve prostheses. The preparation of this tissue for biological valves production consists in fixation with aldehydes, which reduces, but not eliminates, the xenoantigens and the donor cellular material. As a consequence, especially in patients below 65-70 years of age, the employment of pericardium containing valve substitutes is not indicated due to progressive calcification that causes tissue degeneration and recurrence of valve insufficiency. Decellularization with ionic/non-ionic detergents has been proposed as an alternative procedure to prepare aldehyde-/xenoantigen-free pericardium for biological valve manufacturing. In the present contribution we optimized a decellularization procedure that is permissive for seeding and culturing valve competent cells able to colonize and reconstitute a valve-like tissue. A high efficiency cellularization was achieved by forcing cell penetration inside the pericardium matrix using a perfusion bioreactor. Since the decellularization procedure was found not to alter the collagen composition of the pericardial matrix and cells seeded in the tissue constructs consistently grew and acquired the phenotype of 'quiescent' VICs, our investigation sets a novel standard in pericardium application for tissue engineering of 'living' valve implants.

1. INTRODUCTION

Calcific Aortic Valve Disease (CAVD) is one of the cardiac pathologies whose incidence is expected to grow more in the future, due to the worldwide elevation of life expectancy. The current procedures to treat CAVD consist in replacement with mechanical or biological substitutes (Schoen, 2008, Schoen and Gotlieb, 2016). Mechanical valves are manufactured with various materials, especially metal alloys, which provide the advantage to make them structurally and mechanically unmodifiable. Mechanical valve substitutes have, however, a major shortcoming in the need to treat patients with continuous anticoagulant administration to prevent the formation of thrombi (David, 2013). This problem makes these valves unsuitable in elderly patients, who may have a too high risk of bleeding (Head, *et al.*, 2017). Bioprosthetic valves are manufactured with biological materials such as complete valves (from porcine) or animal-derived pericardium (from bovine or porcine) (Head, *et al.*, 2017, Namiri, *et al.*, 2017, Okamoto, *et al.*, 2016, Yap, *et al.*, 2013). The advantage of this type of valve replacements consists in the lack of need to constantly administer anticoagulation therapy. In addition, the adoption of minimally invasive procedures to implant biological valves (the so called Trans Aortic Valves Implants, TAVI) manufactured with animal pericardium, has greatly reduced the operative and post-operative complications, making these devices the preferred option for old patients with CAVD (Nishimura, *et al.*, 2014, Vahanian, *et al.*, 2012).

Irrespective whether pericardial-made prostheses are manufactured as conventionally or minimally invasively implantable devices (Chacko, *et al.*, 2013, Farias, *et al.*, 2012, Johnston, *et al.*, 2015), they are 'xenografts' whose integration in the host fail at mid-long term for lack of a complete immunological compatibility and insufficient fixative detoxification. In fact, the treatment of the animal tissues with aldehyde-based fixatives leaves exogenous immunoreactive biological material (e.g. DNA), xenoantigens (e.g. the 1,3 α-Gal) and aldehyde residues which determine a chronic rejection, resulting into leaflet inflammation/calcification and progressive deterioration of mechanical performance (Carpentier, *et al.*, 1969, Grabenwoger, *et al.*, 1996, Schoen and Levy, 2005, Siddiqui, *et al.*, 2009). Improvement of fixation methods and treatment with agents that detoxify aldehyde residues and xenoantigens have been proposed as strategies to improve the compatibility of the pericardium and reduce its calcification potential (Flameng, *et al.*, 2014,

Guldner, *et al.*, 2009, Leong, *et al.*, 2013, Lim, *et al.*, 2012). Alternatively, decellularization procedures to prepare xenoantigen-free acellular pericardium have been proposed. In these protocols, pericardium is treated with hypotonic buffers and ionic/non-ionic detergents, such as SDS and TritonX-100 (Korossis, *et al.*, 2002, Mirsadraee, *et al.*, 2006, Mirsadraee, *et al.*, 2007). Although these methods maintain a relatively good mechanical performance, abolish the xenoantigen content (Boer, *et al.*, 2012, Gardin, *et al.*, 2015, Ghodsizad, *et al.*, 2014, Roosens, *et al.*, 2016, Wong, *et al.*, 2013), and reduce the tissue immunogenicity (Paola, *et al.*, 2017, Wong, *et al.*, 2016), thus far there has been a limited employment of this approach at an industrial scale for preparation of valve replacement devices (Horke, 2016).

In a previous investigation from our laboratory (Vinci, *et al.*, 2013) we proposed a modification of a standard decellularization method (Mirsadraee, *et al.*, 2006, Mirsadraee, *et al.*, 2007), to obtain a complete cell removal from the human pericardium. In that contribution, the immunological compatibility of the human tissue was demonstrated by subcutaneous transplantation of the decellularized pericardium in immunocompetent mice. The decellularization procedure was also shown not to alter the three dimensional structure and the composition of the extracellular matrix, as well as the tissue mechanical behavior. When the method was tested to assess the compatibility of the animal-derived pericardium for tissue engineering applications (Santoro, *et al.*, 2016), we found a complete removal of animal xenoantigens and the lack of toxic residuals that could impair growing of aortic valve-derived interstitial cells the cell type naturally deputed to valve tissue homeostasis and matrix renewal (Liu, *et al.*, 2007a, Taylor, *et al.*, 2003). Based on these results, in the present contribution we employed a direct perfusion bioreactor to achieve an efficient and homogeneous delivery of valve interstitial cells into the decellularized pericardium (Cioffi, *et al.*, 2008, Wendt, *et al.*, 2003b). Our results showed an optimal growth of valve-derived cells inside the tissue, and a partial maturation as a living leaflet tissue. Compared to less efficient (Dainese, *et al.*, 2012) or technology demanding approaches proposed in the literature to engineer completely recellularized valves (Converse, *et al.*, 2017, Ghodsizad, *et al.*, 2014), our method appears an affordable and easily scalable procedure that may be industrially implemented for generating living valve replacement tissue.

2. MATERIALS AND METHODS

2.1 Porcine pericardium decellularization procedures

Parietal pericardial tissue was dissected from the left ventricle of pig hearts (10±2 months of age) donated by a local slaughterhouse. Two different decellularization procedures were used and compared. The first, named "SDS", was previously described by us (Santoro*, et al.*, 2016), the second, named "Triton", is a refinement of this protocol. Briefly, both procedures start with a first mechanical removal of fat tissue, followed by three 30 min washings in Ca^{2+} and Mg^{2+} free phosphate-buffered saline (PBS) containing protease inhibitors (Aprotinin, 10 KIU mL^{-1}, Trasylol, Bayer, Germany) under continuous agitation. Cell lysis was achieved by osmotic shock treating the tissue with hypotonic buffer (10 mM Tris-HCl; pH 8.0), supplemented with protease inhibitors (Aprotinin, see above), for 16 h, under continuous agitation at 4°C. Samples following the "Triton" protocol were additionally incubated for 24 h in 1% (v/v) Triton X-100 in MilliQ at room temperature under continuous agitation, aiming to break lipid-lipid and lipid-protein interactions. To ensure cell debris removal, both "SDS" and "TRITON" samples were repeatedly washed (3 washes, 30 minutes each, in agitation) with MilliQ and incubated for 24 h in 0.1% (w/v) sodium dodecylsulphate (SDS) in MilliQ at room temperature under continuous agitation. 90 minutes washings in MilliQ, were followed by a 30 min washing in PBS with Ca^{2+} and Mg^{2+} before incubation for 3h at 37°C in a reaction buffer containing 50 U mL^{-1} deoxyribonuclease I from bovine pancreas (DNase, Sigma-Aldrich, Germany) under agitation, serving to nucleic acid material removal. After washing in MilliQ for either 24 (Triton) or 48 (SDS) hours under agitation, samples were, finally, incubated for 72 hours at 4 °C in BASE 128 (AL.CHI.MIA S.r.l.), an EC certified decontamination medium containing an antibiotic/antifungal mixture (Gentamicin, Vancomycin, Cefotaxime and Amphotericin B) approved for employment in Tissue Banking (Gatto*, et al.*, 2013). Mechanical response and biochemical composition of SDS- and Triton-treated decellularized samples were then compared *vs.* the native tissue. Finally, 10 mm diameter circular patches of decellularized pericardium were cut using a biopsy puncher and used for static or dynamic VICs seeding and culture.

2.2 Mechanical characterization

Uniaxial tensile loading (UTL) tests were performed on Native, SDS- and Triton-decellularized pericardium from 10 donors (at least 2 samples per donor). To assess mechanical characteristics rectangular shaped

specimens of 3 mm width were dissected with no preferential orientations, assuming pericardium isotropy. The ends of the specimens were glued with cyanoacrylate adhesive in between of two sheets of sandpaper, to facilitate uniform gripping and to avoid sample slippage. After mounting onto the clamps of the testing machine (MTS System Corporation), samples were preloaded up to 0.01 N and preconditioned through loading-unloading cycles (6 cycles) at 15% maximum strain with an elongation rate of 10 mm/min, until the loading-unloading curves were almost superimposed. After tissue preconditioning, the specimens were preloaded up to 0.01 N. The specimen initial length was measured and UTL test was conducted, at a constant velocity of 10 mm/min, until specimen failure. UTL tests were performed at room temperature and the specimens were maintained hydrated with PBS for the whole test duration. The thickness of each specimen was measured by histological analysis from samples collected next to those used for mechanical tests. Stress was calculated dividing the machine measured force by the resistant area (thickness times width). Strain was calculated by normalizing the machine actuator displacement by the specimen initial length. From the resulting stress-strain curves (σ-ε), the biomechanical properties of the pericardial tissue were described by means of elastic modulus (the σ-ε curve slope) at low (E1) and high (E2) strain, as well as the maximum tensile stress (σ_{max}).

Perfusion tests were employed to evaluate and compare permeability properties of the tissues from 8 donors. The apparatus used to perform the test is constituted of 2 coaxial stainless steel cylindrical parts, and a capillary flow-meter with a resolution of 1 µl. Round-shaped tissue specimens, maintained in PBS at 4°C until the test, were housed into the lower cylinder, over a polyethylene porous filter, and secured between two gaskets. Fluid pressures ranging from 0.74 to 2.21 MPa were obtained using a vertical column filled with different volumes of PBS. After tissue equilibration, time required to filter 5.00 mm^3 for each pressure was measured and the permeability factor K was calculated as defined by the Darcy's Law.

$$K = \frac{Q * L}{A * \Delta P}$$

2.3 Cell and static tissue Culture

Primary aortic valve interstitial cells (VICs) were obtained by enzymatic isolation from explanted porcine aortic valves (10±2 months of age) as previously described (Santoro, *et al.*, 2016). Cells were cultured up to four passages in standard culture dishes, in DMEM (Lonza) containing 150 U mL^{-1} penicillin/streptomycin

(Sigma–Aldrich), 2mM L-glutamine (Sigma–Aldrich) and 10% fetal bovine serum (HyClone, Thermo Scientific). For static culture, the 10 mm diameter pericardium samples were fixed to silicone holders and housed into 6 wells plates. 1.50 E+5 cells were seeded onto each sample, by gently pipetting 50 µl of cell suspension. 2 hours after seeding, 2 ml of complete medium were added to the well, and culture was performed up to 7 days, before dividing each sample in 2 half, respectively, to perform MTT staining or immunofluorescence staining of cross-sections.

2.4 Bioreactor culture

After the decellularization procedure, the pericardium was washed abundantly with sterile PBS to ensure BASE.128 removal. 10 mm diameter patches were obtained using sterile biopsy puncher and were housed into bioreactor chambers, by means of a silicone holder (**Figure 1**), leaving 8 mm diameter of the sample free to allow fluid flow and preventing lateral leakage. After assembly, 10 ml of cell suspension, containing 6.5 E+05 VICs, were injected into each bioreactor using the "injection site" as shown in **Figure 1L.** Oscillatory flow was then started. Flow rate during this phase was optimized in preliminary experiments performed on SDS pericardium, by applying a seeding flow rate of 0.03 mL min^{-1}, 3 mL min^{-1} and 6 mL min^{-1} for 24 hours (Figure S2). On the basis of these results, recellularization procedure was established. This consisted in an initial seeding phase (72 hours) at a high (3 mL min^{-1}) flow rate, followed by a culturing phase, lasting up to 14 days, at a low flow rate (0.03 mL min^{-1}). During cell seeding and the following culturing phases, a reversing flow protocol was applied. This consists in producing an alternate motion of 3 ml medium in both directions across the tissue (**Figure 1L**), that ensures to maintain the patches always in contact with medium and to maximize gas/nutrient supply. Culture medium was partially (6 mL) substituted every 72 hours. At the end of the period, dynamically recellularized samples were harvested, and either destined to MTT assay, or fixed to perform histological sectioning. MTT staining was performed by incubating samples in 400 µL of 1.2 mM MTT [3(4,5- dimethylthiazol-2-yl)-2,5-diphenyltetrazolium bromide] solution at 37°C for 3 h. After incubation, images of both sides of the *in vitro* cellularized pericardium were acquired with Stemi 2000-C Stereo Microscope (Carl Zeiss, Germany).

2.5 Histological sectioning, staining, and immunofluorescence

Pericardium samples, before and after decellularization/recellularization, were fixed in 4% PFA and embedded in paraffin. Histological sections (4 μm thick) were cut and subsequently dewaxed and stained with either Verhoeff-Van Gieson, Hematoxylin and Eosin (H&E) or Masson's trichrome staining and acquired using an Axioscop optical microscope (Carl Zeiss, Germany). Cell distribution in the pericardium was assessed by DAPI (Sigma–Aldrich) nuclei staining. Cell counting was performed by a semi-automated method using ImageJ Software (National Institute of Health, USA). Immunofluorescence analysis were performed on recellularized samples, following unmasking procedure with Sodium Citrate Buffer (10mM, 0.05% Tween-20, pH6.0) at 100°C, permeabilizeation (1% v/v Triton X-100 in PBS-BSA 3% w/v) and incubated with anti-Vimentin (Rabbit, Cell Signalling) and anti-αSMA (Mouse, DAKO) antibody for 16 hours at 4°C. After incubation with secondary antibodies (AlexaFluor 633 and AlexaFluor 488, Life Technologies) for 1 hour at room temperature and DAPI (DAKO) counterstaining, images were acquired with an Apotome fluorescence microscopes (Carl Zeiss, Germany) and Laser Scanning Confocal Microscope (Carl Zeiss, Germany).

2.6 Biochemical characterization and mass spectrometry analysis

Lipids were extracted from homogenized tissue in TNES buffer using the Folch method (Folch, *et al.*, 1957). Cholesterol concentration was measured using an enzymatic assay (Allain, *et al.*, 1974) and normalized for dry tissue weight. For total protein quantification, an extraction buffer containing Tris 0.1M Ph 7.6 and SDS 4% was used. Homogenization was performed with Ultraturrax at 24000 rpm for 30 seconds on ice followed by sonication (10 seconds twice power 6 on ice) and heating at 95°C for 3 min. Equal amounts of proteins from Native, SDS and Triton samples (15ug) were separated by 12% polyacrylamide gel electrophoresis after dilution in Laemmli buffer (Laemmli, 1970) and stained with the Colloidal Blue method (Banfi, *et al.*, 2009). For label-free quantitative mass spectrometry (LC-MS^E), the protein extracts were precipitated with the Protein precipitation kit (Calbiochem, MerckMillipore, Milan, Italy), according to the manufacturer's instructions. Protein pellets were then dissolved in 25 mmol NH4HCO3 containing 0.1% RapiGest (Waters Corporation, Milford, MA, USA) and digested as previously described (Brioschi, *et al.*, 2013). LC-MS^E analysis was performed as previously described and analyzed using Progenesis QIP including normalization of protein abundance considering all the identified proteins (Brioschi, *et al.*, 2014, Roverso, *et al.*, 2016).

Collagen quantification was performed by Sircol soluble collagen (Biocolor) colorimetric assay. Portions (around 45 mg) of frozen tissue (4 donors) were reduced in small pieces by Tissue Pulverizer (Bessman), then collected, weighted and digested over-night at 4 °C in 1 mL of pepsin 0.1 mg/ml and 0.5 M acetic acid solution. The colorimetric reaction was analyzed with absorbance reading at 555 nm on Tecan Infinite M200 PRO spectrophotometer. Absolute values were calculated from interpolation with a curve generated by an internal standard and normalized for dry tissue weight (mg). For Western Blot Analysis, tissue slices from 4 different donors were weighted, minced into small pieces (around 1 mm^3) and homogenized with Ultraturrax in Tris 0.1M Ph 7.6 and SDS 4% buffer as described above. After the sonication, samples were centrifuged at 13000 rpm for 10 minutes and the supernatant was collected. Following protein concentration determination (Pierce™ BCA Protein Assay Kit, Thermo scientific), 2.5 µg of total protein solution into Laemmli buffer was heated at 95 °C and run into a pre-casted 4-12% gradient polyacrylamide gel (BioRad). Collagen Type I solution (2.5 µg) from rat tails (Sigma) was loaded and run as a positive control. Proteins were then transferred to a nitrocellulose membrane (25 mM Tris, 190 mM Glycine, 20% Methanol, SDS 0.02% for 2h at 100 V). Non-specific binding was blocked by incubation with 5% non-fat dried milk in PBS. Overnight incubation at 4 °C with anti-Collagen primary antibodies (Rabbit, Abcam) was followed by incubation for 20 minutes at room temperature with secondary antibodies (LI-COR). Band densitometry was acquired by Odyssey (LI-COR).

2.7 Statistical analysis and data clusterization

All values in bar graphs are represented as mean ± standard error. Differences among experimental groups were assessed by Graph-Pad statistical software. The type of statistical tests and the number of the replicates included in the analyses are specified in the figure legends. Proteomics data clusterization was performed by MeV software with the normalized protein abundance data.

3. RESULTS

3.1 Definition of an optimized pericardium decellularization process for valve tissue engineering applications

Our previous investigations showed that treatment of pericardium with decellularizing agents abolishes the immunological rejection into an immunocompetent environment (Vinci, *et al.*, 2013), and is permissive for cell culturing using valve-derived interstitial cells (Santoro, *et al.*, 2016). Since static cell seeding does not, in general, allow a consistent and reproducible colonization, especially in the inner layers (Dainese, *et al.*, 2012, Namiri, *et al.*, 2017), we speculated that the adoption of a perfusion bioreactor (Wendt, *et al.*, 2003a) might improve efficiency and reproducibility of the process. In the initial part of the work, we therefore designed the strategy to drive cells in the whole pericardium according to conditions already established for synthetic fibrous scaffolds (Santoro, *et al.*, 2010). A direct perfusion bioreactor (U-CUP) was chosen to this aim (Wendt, *et al.*, 2003a). Indeed, the working principle and the performance of this system have been extensively described to enable cell seeding into three-dimensional scaffolds by continuous perfusion of a cell suspension through the scaffold pores. The oscillating direction of the culture medium is automatically controlled by the movement of a syringe pump. Based on the same principle, homogeneous culture conditions and mass transfer (gas and nutrients supply and waste removal) are guaranteed in the whole scaffold volume during long term culture. **Figure 1** shows the phases of tissue preparation from the dissection of the LV parietal pericardium (**A-B**) to the cutting of the 1 cm diameter patches (**D-E**) to be mounting into the holders (**F**), and final bioreactor assembly (**G-K**). A schematic representation of the bioreactor working principle is provided into panel **L**.

For setting the VICs cellularization method, we used pericardium decellularized with the SDS-based protocol previously published by us (Santoro, *et al.*, 2016). As shown in **Figure S2**, the MTT staining of the recellularized patches exhibited a uniform cell distribution on both sides of the patches only in samples that were subject to a 3 ml/min flow rate. On the other hand, the lack of a sufficient cell number in the inner layers prolonging culture time up to 7 days (not shown) suggested a sub-optimal seeding efficiency, likely due to an insufficient permeability of the tissue. In line with this hypothesis, permeability tests showed an insufficient permeability of the SDS-based decellularized tissue that resulted more permeable compared to native tissue only at the highest tested pressures (**Figure 2A**). In order to increase the permeability of the

tissue, thus making it more suitable to be perfused, we set a new decellularization protocol, which included incubation with TritonX-100, a non-ionic detergent that specifically breaks the lipid-lipid and lipid-protein interactions without denaturing the extracellular matrix (Seddon*, et al.*, 2004), after the SDS phase. **Figure 2A** shows that the addition of TritonX-100 to the decellularization procedure determined an increase in the permeability of the tissue *vs.* Native controls at all the tested pressures (fold change 5.08±2.33; 6.05±2.93; 6.66±3.17; 7.56±3.54, mean±SE, n=8, from lowest to highest pressure values as indicated in the figure, respectively). The enhancement in tissue permeability induced by TritonX-100 incubation caused, as estimated by the Darcy low, a one-fold decrease in the hydraulic velocity in the pericardium, both during seeding and culture phases. To monitor the structure of the Triton-treated pericardium, a histological evaluation of the tissues was performed by conventional staining methods. Results of Verhoeff-Van Gieson (**Figure 2B**), hematoxylin/eosin and Masson trichrome staining (**Figure S3**) showed a substantial structural integrity of the matrix fibers in Triton-decellularized *vs.* the two other conditions, although the tissue appeared more swollen, consistently with a higher porosity. In keeping with these results, thickness of the samples treated with the Triton-containing procedure was higher than that of the two controls (fold change 0.99±0.07 and 1.31±0.08; n=10 for SDS and Triton treatments *vs.* Controls, respectively; **Figure 2C**). Finally, to assess whether the addition of Triton to decellularization procedure compromised the tissue mechanical performance, we conducted Uniaxial Tensile Loading (UTL) tests. The three parameters (E1, E2 and σ_{max}) that were derived from traction tests showed a similar behavior in all tested conditions (**Figure 2C**).

3.2 Biochemical characterization of the decellularized characterization reveals complete removal of cellular proteins without affecting extracellular matrix components

The previous results showed that addition of an incubation step with Triton to the SDS-based decellularization method increased permeability without jeopardizing the structure and the mechanical resistance of the pericardial matrix. On the other hand, since the composition of the extracellular matrix is crucial to ensure an optimal growth of valve cells, we investigated the effects of the decellularization method on the total proteins and collagen content. We completed this analysis with the assessment of the lipids components and a quantitative mass spectrometry-based investigation. The results of total protein quantification indicated a significant decrease into either SDS- and Triton-based decellularization methods

content, especially in the low molecular weight component (**Figure 3A**). This decrease was similar in Triton- and SDS-based treatments, suggestive of a similar efficiency of the two methods at removing cellular proteins.

The analysis of collagen content by Sircol Red and Western blotting showed that the total amount of collagen I, the main pericardium matrix component, was not reduced by none of the treatments (**Figure 3B**). Furthermore, the mass spectrometry approach followed by unsupervised clusterization analysis (**Figures 3C and D**) indicated a change in the relative protein composition between the untreated and the treated samples. This determined an increase in the relative amount of collagenous structural matrix component (with exception of Col14A1), and a parallel reduction of cellular proteins and proteoglycans matrix component (see **Tables 1** and **S1** for data on relative abundance of the matrix related protein components and description of the identifiable proteins, respectively). Finally, the assay of cholesterol content revealed a significantly lipid decrease only in Triton-treated samples (**Figure 3B**). Taken together, these results suggest that Triton-based decellularization does not affect the major structural and mechanical component of the tissue, but determines an increased tissue permeability by efficient lipids removal compared to the SDS treatment.

3.3 Perfusion-driven seeding ensures physiologic growth of valve interstitial cells inside the decellularized pericardium

The lower local velocity in the inner layers of the pericardium was supposed to favor a more homogeneous and efficient cell seeding, by better supporting cell adhesion and survival, and reducing the shear stress on the cells, without jeopardizing mass transfer inside the tissue. A final recellularization procedure was therefore established including an initial VICs oscillatory seeding phase for three days at 3 ml/min flow rate(v=1 mm/s), followed by a tissue maturation phase (still under oscillatory flow) at 0.03 ml/min (v=10 μm/s) (Santoro*, et al.*, 2012). Under these conditions, according to MTT staining, a constant VICs increase occurred inside the entire pericardium volume (**Figure 4A**). The analysis of transversal tissue sections of the recellularized Triton-treated pericardium, followed by nuclei counting, confirmed a substantial and constant VICs growth (**Figure 4 B-C**). Remarkably, the presence of cells inside the tissue indicated the robustness of the recellularization protocol. To confirm the effectiveness of the recellularization process, an analysis of the VICs phenotype inside the recellularized tissue was performed by immunofluorescence. In this analysis, staining with antibodies recognizing Vimentin and αSMA, two markers of VICs and 'activated' VICs under

standard culture conditions (Porras, *et al.*, 2017) (**Figure S4**) were performed to discriminate between cells that may have a self-renewal *vs.* a *pro*-pathologic phenotype. **Figure 5A** shows representative images of the cells inside the pericardium at the three considered time-points. In addition to reveal a robust growing of the cells that tended to progressively invade the tissue from the surface, an evident downregulation of the αSMA was observed, especially in cells colonizing the inner portion (**Figure 5B**). These results are consistent with a growth of the cells inside the decellularized matrix with a quiescent phenotype (Porras, *et al.*, 2017).

4. DISCUSSION

The results of the present investigation show an unprecedented efficiency of cell seeding inside decellularized pericardium to generate fully cellularized valve-like tissue endowed with a self-renewal potential. Although the approach is not novel, our work sets a new standard in valve tissue engineering compared to existing literature. In fact, previous investigations showed insufficient cells growth throughout the tissue depth due to the limited cell penetration (Dainese, *et al.*, 2012, Ghodsizad, *et al.*, 2014, Liu, *et al.*, 2016). In our view, the key elements that contributed to this results were: the ***i)*** adoption of an optimized decellularization procedure based on sequential incubation of the pericardium into SDS and TritonX-100 solutions and ***ii)*** the employment of a standardized cellularization procedure based on oscillatory forced perfusion, which enabled a full penetration of cells inside the tissue, followed by a phase of tissue maturation.

In two previous reports published by our group (Santoro, *et al.*, 2016, Vinci, *et al.*, 2013), a SDS-based decellularization process was adopted to remove cellular content and improve the immunocompatibility of human- and animal-derived pericardium for valve tissue manufacturing. While this method proved effective for removing xenoantigens and reduce the foreign body reaction after tissue transplantation, it was not yet thoroughly tested to produce an acellular scaffold suitable for valve engineering applications. Compared to the studies originally reporting the pericardium decellularization methods (Mirsadraee, *et al.*, 2006, Mirsadraee, *et al.*, 2007), we focused our attention to demonstrate the acquisition of permeability by the tissue following decellularization. In fact, we reasoned that only by enabling a substantial mass transport, able to vehicle cells and nutrients/oxygen inside the cell free tissue over the culture time, we might achieve an effective colonization and maintenance of the cells in the inner layers. In one of our reports, in particular, we already in part substantiated the observation that the SDS-based decellularization increases the permeability of the pericardium, even though we did not test appropriately this issue (Santoro, *et al.*, 2016). The results presented here (**Figure 2A**) extend those observations by showing that treatment with only SDS did not increase significantly the permeability of the pericardium if not at the highest applied pressures, thus making the tissue unsuitable to be efficiently recellularized at low pressure values. In keeping with this result, the bioreactor-based recellularization of the tissue decellularized with the SDS method was not

efficient to ensure a robust penetration of the cells inside pericardium in a wide range of applied flow rates (**Figure S2**), thus calling for a further refinement of the decellularization method.

The addition of an incubation step with a solution containing TritonX-100 helped us to improve the decellularization efficiency by removing part of the lipids present in the tissue (**Figure 3B**). By destroying the interactions with proteins (Seddon, *et al.*, 2004), the removal of lipids from the tissue caused a remarkable increase in permeability compared to native and SDS samples (**Figure 2A**). On the other hand, the evidence that the Triton method did not reduce the collagen content and the resistance to traction (**Figures 2-3** and **Table 1**) shows that the method is potentially suitable to ensure a maximal resistance to mechanical stress typical of the opening/closing cycles of the natural valve. Thus, in addition to completely removing the α-GAL xenoantigen ((Santoro, *et al.*, 2016) and **Figure 2B**), and reducing the propensity to induce calcification due to extensive lipids removal (Roosens, *et al.*, 2016, Rossi, *et al.*, 1990), our method preserves the innate resistance of the pericardium tissue to mechanical stress and enables efficient cellularization with recipient-derived cells, which would not be rejected as non-self by recipient hosts.

As discussed in the previous sections, the increase in tissue permeability was only one of the two critical features to succeed in ensuring a substantial growth of valve derived-cells inside the pericardium. In fact, the seeding performed using simple static culture did not allow consistent and controllable VICs homing into the decellularized tissue (Santoro, *et al.*, 2016) (**Figure S2**). Based on our previous experience on perfusion-based cellularization of large scaffolds (Santoro, *et al.*, 2010), and on the reported advantage of mass transport through scaffolds to generate large engineered tissues (Wendt, *et al.*, 2005, Wendt, *et al.*, 2003a), we exploited the characteristics of a perfusion culture system to force penetration of VICs inside the pericardium matrix and observe, for the first time, their behavior. Remarkably, our results (**Figure 5**) indicated a marked downregulation of the activated VICs marker αSMA only in cells that grew inside the matrix and not those covering the two surfaces. While this result is consistent with the reversibility of VICs activation process (Schroer and Merryman, 2015), it also highlights the fundamental role of these cells as possible 'mechanosensors', which may act in detection of local matrix stiffness at the crossroad between self-renewal or pathologic progression of valve tissue (Chen, *et al.*, 2009, David Merryman, 2010, Fisher, *et al.*, 2013, Liu, *et al.*, 2007b, Ma, *et al.*, 2017, Wang, *et al.*, 2014, Yip, *et al.*, 2009). In this respect, it will be interesting to determine whether cells colonizing the inner pericardium layers will contribute to novel matrix

deposition and to mechanical maturation of the matrix itself, and thus to establish specific cell mechanics criteria to be met in order to manufacture artificial valve tissue endowed with self-regeneration capacity (Parvin Nejad*, et al.*, 2016, Pesce and Santoro, 2017).

In conclusion, the present work establish an efficient and potentially industrially scalable method to obtain a substantial growth of valve competent cells in animal-derived pericardium with the potential to be employed in the manufacturing of living tissue for valve replacement therapies.

Conflicts of interest

The Authors declare no conflicts of interest

Acknowledgements

The Authors are indebted to Mr. Luigi Colombo for the supply of porcine pericardial samples from a local slaughterhouse and to Prof. Fulvio Gandolfi (University of Milano) for help with dissection of the ventricular parietal pericardium. The present work was funded from an institutional grant (Ricerca Corrente; 5 per mille) to MP and, in part, by a young investigator grant, issued to RS (GR-2011-02348707).

References

Allain CC, Poon LS, Chan CSG*, et al.* 1974, Enzymatic Determination of Total Serum Cholesterol, *Clinical Chemistry*, **20** (4): 470.

Banfi C, Brioschi M, Barcella S*, et al.* 2009, Proteomic analysis of human low-density lipoprotein reveals the presence of prenylcysteine lyase, a hydrogen peroxide-generating enzyme, *PROTEOMICS*, **9** (5): 1344-1352.

Boer U, Lohrenz A, Klingenberg M*, et al.* 2012, The effect of detergent-based decellularization procedures on cellular proteins and immunogenicity in equine carotid artery grafts, *Biomaterials*, **32** (36): 9730-9737.

Brioschi M, Eligini S, Crisci M*, et al.* 2014, A mass spectrometry-based workflow for the proteomic analysis of in vitro cultured cell subsets isolated by means of laser capture microdissection, *Analytical and Bioanalytical Chemistry*, **406** (12): 2817-2825.

Brioschi M, Lento S, Tremoli E*, et al.* 2013, Proteomic analysis of endothelial cell secretome: a means of studying the pleiotropic effects of Hmg-CoA reductase inhibitors, *Journal of proteomics*, **78**: 346-361.

Carpentier A, Lemaigre G, Robert L*, et al.* 1969, Biological factors affecting long-term results of valvular heterografts, *The Journal of thoracic and cardiovascular surgery*, **58** (4): 467-483.

Chacko SJ, Ansari AH, McCarthy PM*, et al.* 2013, Prosthesis-patient mismatch in bovine pericardial aortic valves: evaluation using 3 different modalities and associated medium-term outcomes, *Circulation Cardiovascular imaging*, **6** (5): 776-783.

Chen JH, Yip CY, Sone ED*, et al.* 2009, Identification and characterization of aortic valve mesenchymal progenitor cells with robust osteogenic calcification potential, *Am J Pathol*, **174** (3): 1109-1119.

Cioffi M, Kuffer J, Strobel S*, et al.* 2008, Computational evaluation of oxygen and shear stress distributions in 3D perfusion culture systems: macro-scale and micro-structured models, *Journal of biomechanics*, **41** (14): 2918-2925.

Converse GL, Buse EE, Neill KR*, et al.* 2017, Design and efficacy of a single-use bioreactor for heart valve tissue engineering, *Journal of Biomedical Materials Research Part B: Applied Biomaterials*, **105** (2): 249-259.

Dainese L, Guarino A, Burba I*, et al.* 2012, Heart valve engineering: decellularized aortic homograft seeded with human cardiac stromal cells, *J Heart Valve Dis*, **21** (1): 125-134.

David Merryman W. 2010, Mechano-potential etiologies of aortic valve disease, *Journal of Biomechanics*, **43** (1): 87-92.

David TE. 2013, Surgical treatment of aortic valve disease, *Nat Rev Cardiol*, **10** (7): 375-386.

Farias FR, da Costa FD, Balbi Filho EM*, et al.* 2012, Aortic valve replacement with the Cardioprotese Premium bovine pericardium bioprosthesis: four-year clinical results, *Interactive cardiovascular and thoracic surgery*, **15** (2): 229-234.

Fisher C, Chen J, Merryman WD. 2013, Calcific nodule morphogenesis by heart valve interstitial cells is strain dependent, *Biomech Model Mechanobiol*, **12** (1): 5-17.

Flameng W, Rega F, Vercalsteren M*, et al.* 2014, Antimineralization treatment and patient-prosthesis mismatch are major determinants of the onset and incidence of structural valve degeneration in bioprosthetic heart valves, *The Journal of thoracic and cardiovascular surgery*, **147** (4): 1219-1224.

Folch J, Lees M, Stanley GHS. 1957, A SIMPLE METHOD FOR THE ISOLATION AND PURIFICATION OF TOTAL LIPIDES FROM ANIMAL TISSUES, *Journal of Biological Chemistry*, **226** (1): 497-509.

Gardin C, Ricci S, Ferroni L*, et al.* 2015, Decellularization and Delipidation Protocols of Bovine Bone and Pericardium for Bone Grafting and Guided Bone Regeneration Procedures, *PloS one*, **10** (7): e0132344.

Gatto C, Giurgola L, D'Amato Tothova J. 2013, A suitable and efficient procedure for the removal of decontaminating antibiotics from tissue allografts, *Cell and tissue banking*, **14** (1): 107-115.

Ghodsizad A, Bordel V, Wiedensohler H*, et al.* 2014, Magnetically guided recellularization of decellularized stented porcine pericardium-derived aortic valve for TAVI, *ASAIO journal (American Society for Artificial Internal Organs : 1992)*, **60** (5): 582-586.

Grabenwoger M, Sider J, Fitzal F*, et al.* 1996, Impact of glutaraldehyde on calcification of pericardial bioprosthetic heart valve material, *Ann Thorac Surg*, **62** (3): 772-777.

Guldner NW, Jasmund I, Zimmermann Hr*, et al.* 2009, Detoxification and Endothelialization of Glutaraldehyde-Fixed Bovine Pericardium With Titanium Coating, *Circulation*, **119** (12): 1653-1660.

Head SJ, Celik M, Kappetein AP. 2017, Mechanical versus bioprosthetic aortic valve replacement, *Eur Heart J*.

Horke A. 2016, Decellularization of aortic valves: only time will tell, *Eur J Cardiothorac Surg*, **49** (3): 707-708.

Johnston DR, Soltesz EG, Vakil N*, et al.* 2015, Long-term durability of bioprosthetic aortic valves: implications from 12,569 implants, *The Annals of thoracic surgery*, **99** (4): 1239-1247.

Korossis SA, Booth C, Wilcox HE*, et al.* 2002, Tissue engineering of cardiac valve prostheses II: biomechanical characterization of decellularized porcine aortic heart valves, *J Heart Valve Dis*, **11** (4): 463-471.

Laemmli UK. 1970, Cleavage of structural proteins during the assembly of the head of bacteriophage T4, *Nature*, **227** (5259): 680-685.

Leong J, Munnelly A, Liberio B*, et al.* 2013, Neomycin and carbodiimide crosslinking as an alternative to glutaraldehyde for enhanced durability of bioprosthetic heart valves, *Journal of biomaterials applications*, **27** (8): 948-960.

Lim H-G, Kim SH, Choi SY*, et al.* 2012, Anticalcification effects of decellularization, solvent, and detoxification treatment for genipin and glutaraldehyde fixation of bovine pericardium, *European Journal of Cardio-Thoracic Surgery*, **41** (2): 383-390.

Liu AC, Joag VR, Gotlieb AI. 2007a, The Emerging Role of Valve Interstitial Cell Phenotypes in Regulating Heart Valve Pathobiology, *The American Journal of Pathology*, **171** (5): 1407-1418.

Liu AC, Joag VR, Gotlieb AI. 2007b, The emerging role of valve interstitial cell phenotypes in regulating heart valve pathobiology, *The American journal of pathology*, **171** (5): 1407-1418.

Liu ZZ, Wong ML, Griffiths LG. 2016, Effect of bovine pericardial extracellular matrix scaffold niche on seeded human mesenchymal stem cell function, *Scientific reports*, **6**: 37089.

Ma H, Killaars AR, DelRio FW*, et al.* 2017, Myofibroblastic activation of valvular interstitial cells is modulated by spatial variations in matrix elasticity and its organization, *Biomaterials*, **131**: 131-144.

Mirsadraee S, Wilcox HE, Korossis SA*, et al.* 2006, Development and characterization of an acellular human pericardial matrix for tissue engineering, *Tissue Eng*, **12** (4): 763-773.

Mirsadraee S, Wilcox HE, Watterson KG*, et al.* 2007, Biocompatibility of acellular human pericardium, *The Journal of surgical research*, **143** (2): 407-414.

Namiri M, Ashtiani MK, Mashinchian O*, et al.* 2017, Engineering natural heart valves: possibilities and challenges, *Journal of tissue engineering and regenerative medicine*, **11** (5): 1675-1683.

Nishimura RA, Otto CM, Bonow RO*, et al.* 2014, 2014 AHA/ACC Guideline for the Management of Patients With Valvular Heart Disease: a report of the American College of Cardiology/American Heart Association Task Force on Practice Guidelines, *Circulation*, **129** (23): e521-643.

Okamoto Y, Yamamoto K, Yoshii S. 2016, Early and Late Outcomes of Aortic Valve Replacement Using Bioprosthetic Versus Mechanical Valve in Elderly Patients: A Propensity Analysis, *Journal of cardiac surgery*, **31** (4): 195-202.

Paola A, Laura I, Francesca F*, et al.* 2017, In vitro comparative assessment of decellularized bovine pericardial patches and commercial bioprosthetic heart valves, *Biomedical Materials*, **12** (1): 015021.

Parvin Nejad S, Blaser MC, Santerre JP*, et al.* 2016, Biomechanical conditioning of tissue engineered heart valves: Too much of a good thing?, *Advanced drug delivery reviews*, **96**: 161-175.

Pesce M, Santoro R. 2017, Feeling the right force: How to contextualize the cell mechanical behavior in physiologic turnover and pathologic evolution of the cardiovascular system, *Pharmacology & Therapeutics*, **171**: 75-82.

Porras AM, van Engeland NCA, Marchbanks E*, et al.* 2017, Robust Generation of Quiescent Porcine Valvular Interstitial Cell Cultures, *Journal of the American Heart Association*, **6** (3).

Roosens A, Somers P, De Somer F*, et al.* 2016, Impact of Detergent-Based Decellularization Methods on Porcine Tissues for Heart Valve Engineering, *Annals of biomedical engineering*, **44** (9): 2827-2839.

Rossi MA, Braile DM, Teixeira MD*, et al.* 1990, Lipid extraction attenuates the calcific degeneration of bovine pericardium used in cardiac valve bioprostheses, *J Exp Pathol (Oxford)*, **71** (2): 187-196.

Roverso M, Brioschi M, Banfi C*, et al.* 2016, A preliminary study on human placental tissue impaired by gestational diabetes: a comparison of gel-based versus gel-free proteomics approaches, *European journal of mass spectrometry (Chichester, England)*, **22** (2): 71-82.

Santoro R, Consolo F, Spiccia M*, et al.* 2016, Feasibility of pig and human-derived aortic valve interstitial cells seeding on fixative-free decellularized animal pericardium, *Journal of Biomedical Materials Research Part B: Applied Biomaterials*, **104** (2): 345-356.

Santoro R, Krause C, Martin I*, et al.* 2012, On-line monitoring of oxygen as a non-destructive method to quantify cells in engineered 3D tissue constructs, *Journal of tissue engineering and regenerative medicine*, **6** (9): 696-701.

Santoro R, Olivares AL, Brans G*, et al.* 2010, Bioreactor based engineering of large-scale human cartilage grafts for joint resurfacing, *Biomaterials*, **31** (34): 8946-8952.

Schoen FJ. 2008, Evolving concepts of cardiac valve dynamics: the continuum of development, functional structure, pathobiology, and tissue engineering, *Circulation*, **118** (18): 1864-1880.

Schoen FJ, Gotlieb AI. 2016, Heart valve health, disease, replacement, and repair: a 25-year cardiovascular pathology perspective, *Cardiovascular pathology : the official journal of the Society for Cardiovascular Pathology*, **25** (4): 341-352.

Schoen FJ, Levy RJ. 2005, Calcification of tissue heart valve substitutes: progress toward understanding and prevention, *The Annals of thoracic surgery*, **79** (3): 1072-1080.

Schroer AK, Merryman WD. 2015, Mechanobiology of myofibroblast adhesion in fibrotic cardiac disease, *J Cell Sci*, **128** (10): 1865-1875.

Seddon AM, Curnow P, Booth PJ. 2004, Membrane proteins, lipids and detergents: not just a soap opera, *Biochimica et biophysica acta*, **1666** (1-2): 105-117.

Siddiqui RF, Abraham JR, Butany J. 2009, Bioprosthetic heart valves: modes of failure, *Histopathology*, **55** (2): 135-144.

Taylor PM, Batten P, Brand NJ*, et al.* 2003, The cardiac valve interstitial cell, *Intern J Biochem Cell Biol*, **35** (2): 113-118.

Vahanian A, Alfieri O, Andreotti F*, et al.* 2012, Guidelines on the management of valvular heart disease (version 2012), *European heart journal*, **33** (19): 2451-2496.

Vinci MC, Tessitore G, Castiglioni L*, et al.* 2013, Mechanical Compliance and Immunological Compatibility of Fixative-Free Decellularized/Cryopreserved Human Pericardium, *PLoS ONE*, **8** (5): e64769.

Wang H, Leinwand LA, Anseth KS. 2014, Cardiac valve cells and their microenvironment - insights from in vitro studies, *Nat Rev Cardiol*, **11** (12): 715-727.

Wendt D, Jakob M, Martin I. 2005, Bioreactor-based engineering of osteochondral grafts: from model systems to tissue manufacturing, *Journal of Bioscience and Bioengineering*, **100** (5): 489-494.

Wendt D, Marsano A, Jakob M, *et al.* 2003a, Oscillating perfusion of cell suspensions through three-dimensional scaffolds enhances cell seeding efficiency and uniformity, *Biotechnology and Bioengineering*, **84** (2): 205-214.

Wendt D, Marsano A, Jakob M, *et al.* 2003b, Oscillating perfusion of cell suspensions through three-dimensional scaffolds enhances cell seeding efficiency and uniformity, *Biotechnology and bioengineering*, **84** (2): 205-214.

Wong ML, Wong JL, Athanasiou KA, *et al.* 2013, Stepwise solubilization-based antigen removal for xenogeneic scaffold generation in tissue engineering, *Acta Biomaterialia*, **9** (5): 6492-6501.

Wong ML, Wong JL, Vapniarsky N, *et al.* 2016, In vivo xenogeneic scaffold fate is determined by residual antigenicity and extracellular matrix preservation, *Biomaterials*, **92**: 1-12.

Yap KH, Murphy R, Devbhandari M, *et al.* 2013, Aortic valve replacement: is porcine or bovine valve better?, *Interact Cardiovasc Thorac Surg*, **16** (3): 361-373.

Yip CY, Chen JH, Zhao R, *et al.* 2009, Calcification by valve interstitial cells is regulated by the stiffness of the extracellular matrix, *Arterioscler Thromb Vasc Biol*, **29** (6): 936-942.

Figure Legends.

Figure 1. Description of the pericardium processing. After the dissection from the pig hearts left ventricles (**A**), the parietal pericardium was further dissected and decellularized as described in the materials and methods (**B-C**). It is evident the change in the color of the tissue due to removal of blood and cell content. Patches with a 1cm diameter of were cut from the tissue with a biopsy puncher (**D**) and then mounted into the bioreactor holders (**E-H**). After joining the holders to the bioreactors circuits (**I**), the assembled bioreactors were placed onto a rack for transfer into the culture incubator, and connection to the peristaltic pump (**J-K**). Note in panel **J** the injection of the cells into the bioreactor that was operated by a syringe. (**L**) Schematic representation of the bioreactor working principle. The pericardium sample is clamped in the chamber, allowing medium to flow only through the patch. Culture medium and cell suspension are injected through the injection site, and the alternate reverse flow is controlled by a syringe pump.

Figure 2. Permeability, structural, antigenic and mechanical characterization of the pericardium. (**A**) Permeability of the tissue was plotted as a function of the applied pressure. The SDS-based decellularization determined an increase in permeability of the tissue compared to the untreated pericardium only at the highest pressure levels. By contrast, the Triton-treated pericardium exhibited higher values at all the considered pressures compared to Native or SDS-decellularized samples. Statistical significance of grouped data comparison was determined by two ways ANOVA with Bonferroni post-hoc analysis ($P < 0.05$ indicated by *, n=8) and by pairwise Student's t-test for comparisons at each pressure level ($P < 0.05$ indicated by #, n=8) (n=8). Data are plotted as means with standard errors. (**B**) Histological appearance and antigenic characterization of Native, SDS-treated and Triton-treated pericardium. Upper panels show the results of Verhoeff/Van Gieson staining of the tissues (arrows indicate cell nuclei), while the lower panels the immunofluorescence staining with the nuclear dye DAPI and an antibody recognizing the pig αGAL (Santoro*, et al.*, 2016). Note the complete removal of the nuclei in the decellularized samples in all panels, and that of the major pig xenoantigen (green fluorescence) in the lower. (**C**) The morphometric evaluation of the samples thickness (graph **a**) revealed a significant increase in the Triton-treated samples compared to the other two conditions, possibly due to increase in tissue porosity and permeability. Data (n=10 donors) are plotted as means with standard errors. Mechanical characterization by UTL tests (graphs **b-d**) allowed to determine the resistance to traction of the native and the decellularized samples. None of the parameters in these tests differed significantly between treatments. This, in keeping with our previous results (Santoro*, et al.*, 2016, Vinci*, et al.*, 2013) indicates that the two decellularization methods did not affect pericardium mechanical characteristics. * indicates by $P < 0.05$ by one way ANOVA (repeated measures) with a Newman Keuls post-hoc comparison (n=10).

Figure 3. Protein and lipid analysis of decellularized pericardium. (**A**) SDS-PAGE of total proteins extracted from native, SDS- and Triton-decellularized pericardium. As it is evident by the electrophoretic run and the protein quantification by Colloidal Blue, a similar extent proteins removal (especially in the low

molecular weight range) was observed by both decellularization methods. * indicates $P < 0.05$ by one way ANOVA (repeated measures) with a Newman Keuls post-hoc comparison (n=3). (**B**) Collagen content evaluation performed by Sircol (upper graph) and Western Analysis (middle picture) showed that the two decellularization methods did not impact on the overall collagen content. By contrast, the cholesterol content was sharply reduced by the Triton-, but not the SDS-, based decellularization method. * indicates by $P < 0.05$ by one way ANOVA (repeated measures) with a Newman Keuls post-hoc comparison (n=4 and 6 for Sircol red collagen determination and cholesterol content, respectively). (**C**) The heatmap shows the results of the unsupervised clusterization analysis of all the detectable proteins by quantitative mass-spectrometry analysis. This showed a clearly different protein representation in SDS and Triton-treated *vs.* the untreated samples. The analysis indicated the existence of two clusters in which proteins were overrepresented in decellularized *vs.* native samples and vice versa (See also **Table S1** for a full detail on proteins identity and significance of data comparison). (**D**) Graphic representation of the clusterized data of the protein relative abundance representing extracellular matrix components (details in **Table 1**), as detected by mass-spectrometry in pericardial samples. The protein identity is indicated according to ENSEMBL and UNIPROT databases annotation. The heatmap shows that decellularization treatment caused a variation in the abundance of matrix-specific proteins, with a substantial elevation of the collagen species (except for Collagen12), and an abatement of the proteoglycan content.

Figure 4. Adoption of a bioreactor-based perfusion cell seeding enhances cellularization efficiency and growth of VICs in Triton-treated pericardium. (**A**) MTT staining of semilunar Triton-treated pericardial patches cellularized and matured in perfusion bioreactor. The increment in MTT color staining on both sides of the patches denotes a substantial growth of cells over the time of tissue culture. (**B-C**) DAPI staining in transversal sections of recellularized patches was employed to assess VICs growth inside the recellularized tissue. Cells quantification denoted a robust and constant increment of the cell number in the patches. * indicates by $P < 0.05$ by one way ANOVA (repeated measures) with a Newman Keuls post-hoc comparison (n=4).

Figure 5. Histological and immunofluorescence-based characterization of the recellularized pericardium patches. (**A**) Histological appearance of the Triton-treated recellularized pericardium during the course of maturation in the perfusion bioreactor as detected by Hematoxylin/Eosin, Masson's Trichrome and Verhoeff/Van Gieson staining (upper, middle and lower panels, respectively). The pictures show that cells progressively invade the tissue from the two surfaces. Note that none of the staining methods revealed a change in the structure of the collagen fibers at any time during the course of tissue maturation inside the culture system. (**B-D**) Low and high magnification of confocal-based imaging of porcine VICs colonizing the pericardium at different culture time points (panel **B**: 3 days; panel **C**: 7 days; panel **D**: 14 days). Sections were stained with antibodies recognizing Vimentin (red fluorescence) and αSMA (green fluorescence). As shown in the panels, the culture into the oscillating perfusion system determined a progressive increase in the cell content inside the tissue. Interestingly, cells differed for the expression of αSMA depending on their

position in the constructs, with high levels in cells adhering to construct surface (white arrows) and low or absent level in cells found inside the tissue (blue arrows). This latter finding suggests that VICs undergo a transition from an activated to a quiescent phenotype when surrounded by pericardium matrix.

Table 1. Normalized abundance (NA: mean and standard deviation) of the extracellular matrix-related proteins identified by mass spectrometry in Native, SDS- and Triton-treated pericardial samples (data also clusterized in **Figure 3D**). Protein identity is indicated according to ENSEMBL/UNIPROT databases. Data are representative of 3 independent donors. Pairwise comparisons significance was calculated by ANOVA using the Progenesis Software.

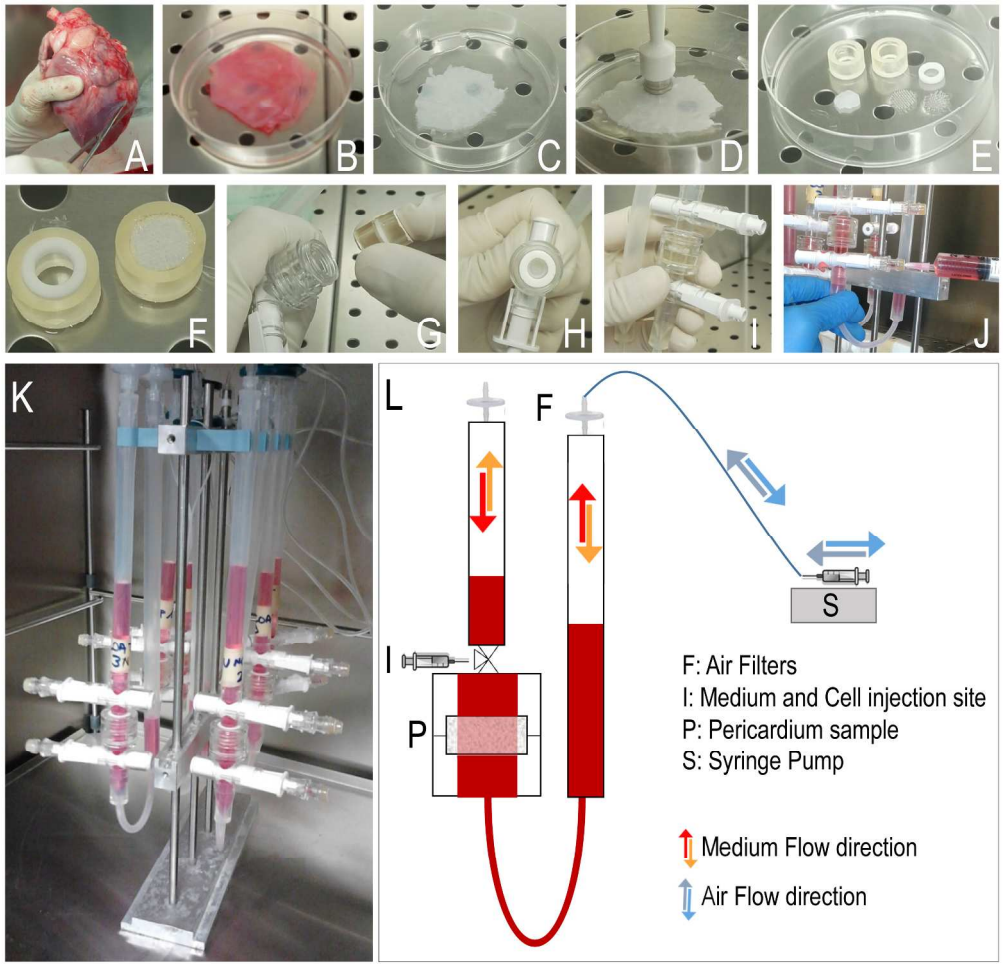

figure 1

235x226mm (300 x 300 DPI)

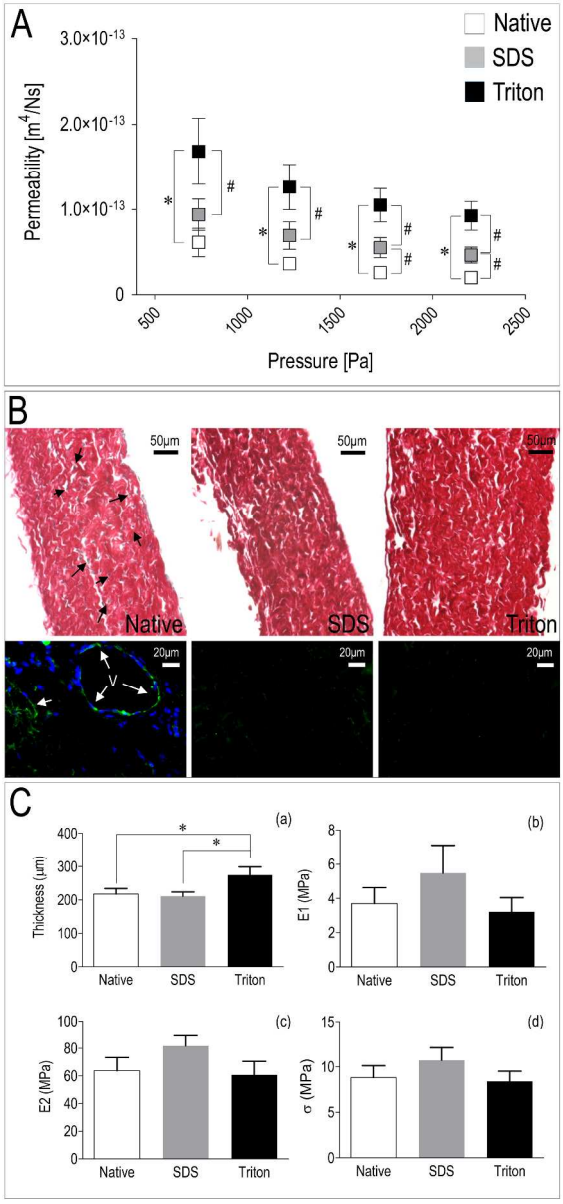

figure 2

193x415mm (300 x 300 DPI)

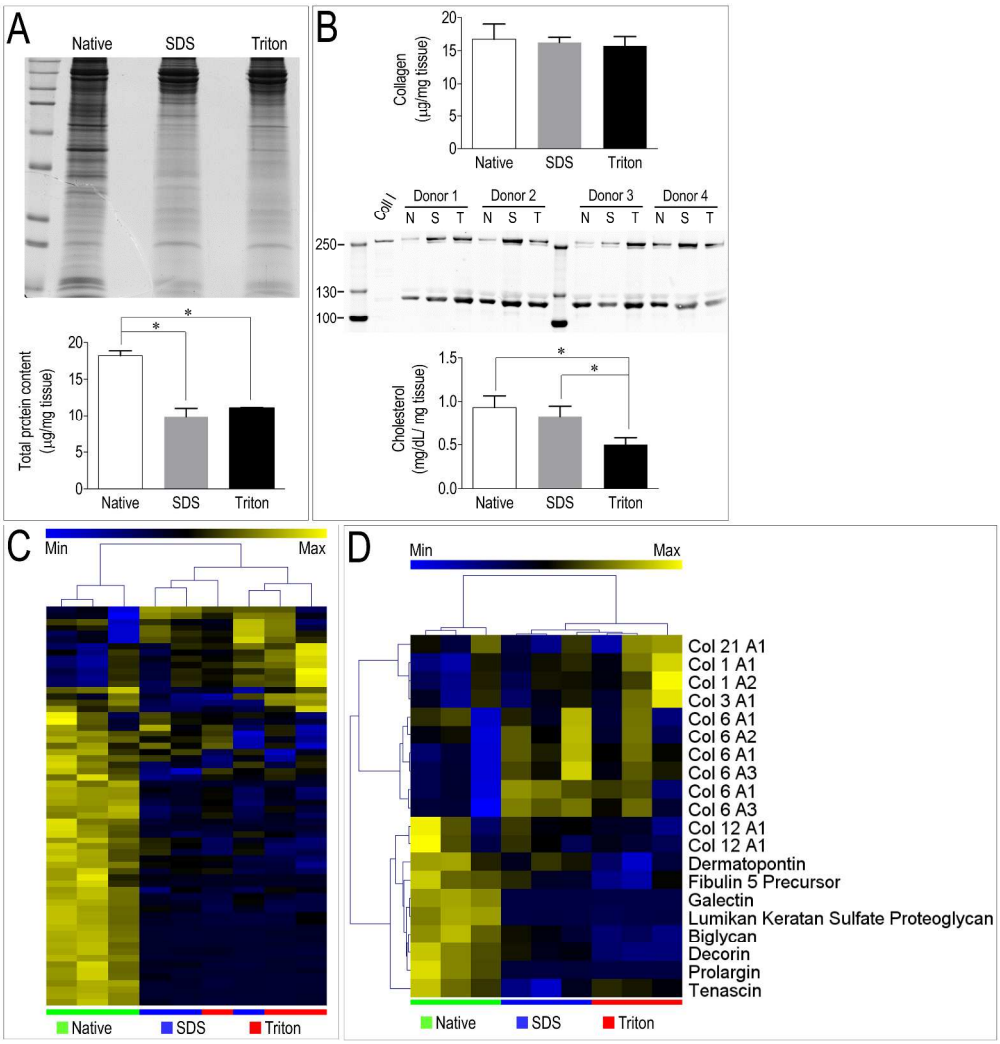

figure 3

318x331mm (300 x 300 DPI)

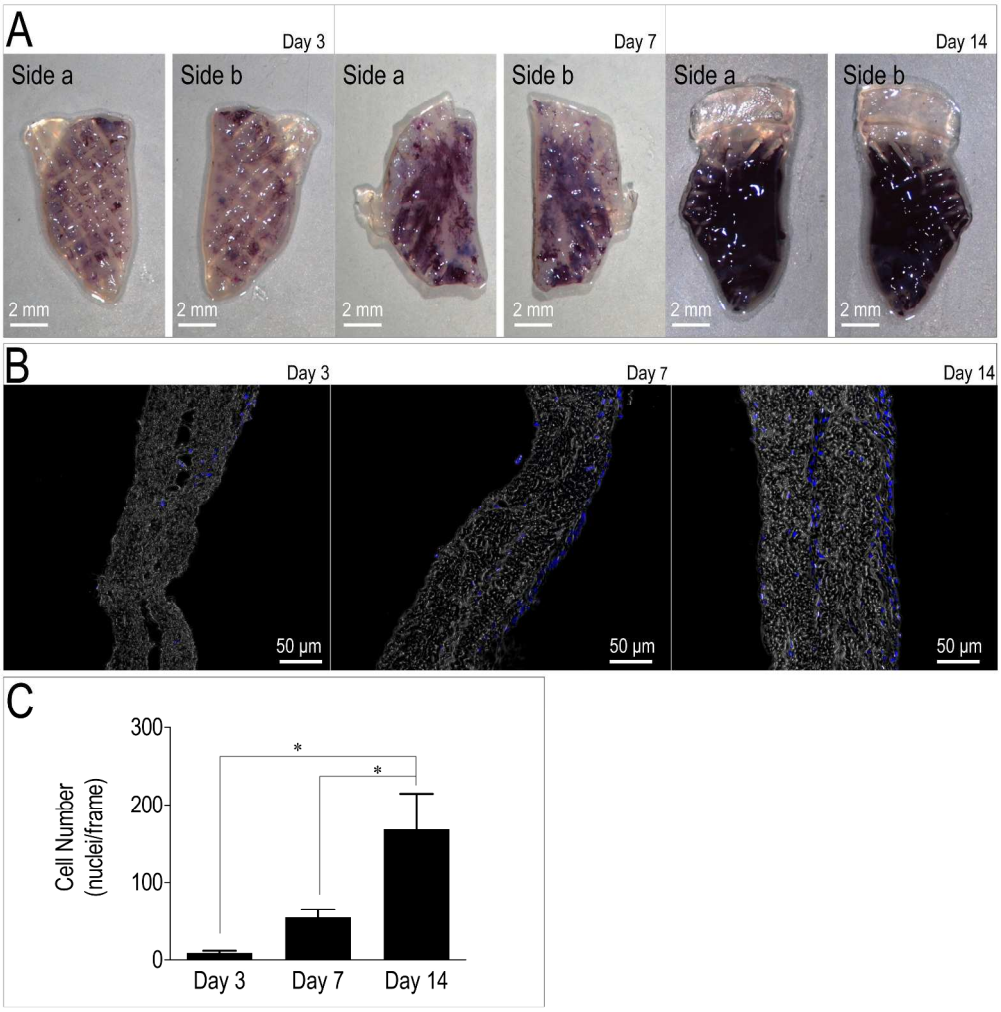

figure 4

279x281mm (300 x 300 DPI)

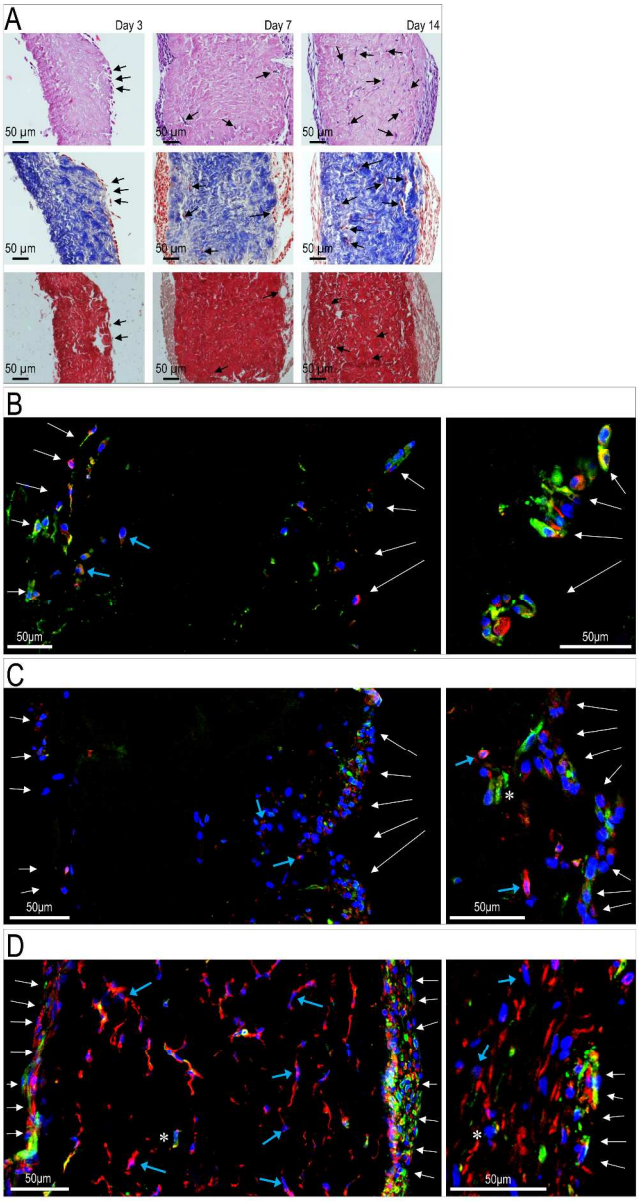

figure 5

279x524mm (300 x 300 DPI)

Accession	Protein ID	Native (mean NA)	Native (S.D)	SDS (mean NA)	SDS (S.D.)	Triton (mean NA)	Triton (S.D.)	Native *vs.* SDS	Native *vs.* Triton	SDS *vs.* Triton
K7GP55	Biglycan	16863.1	2501.2	8261.6	1429.6	4580.7	732.8	<0.0001	<0.0001	<0.0001
I3LJX2	Col 1 A1	1676.1	324.8	1954.2	168.2	2383.4	494.6	<0.05	<0.001	n/s
F1SFA7	Col 1 A2	12986.9	2061.9	14074.0	1346.0	17413.4	4199.9	n/s	<0.001	n/s
F1RQI0	Col 12 A1	15959.8	6935.0	12952.7	1646.1	10061.5	1651.6	n/s	<0.05	<0.001
F1RQI2	Col 12 A1	1665.2	1061.8	981.2	378.2	742.6	150.2	n/s	n/s	n/s
F1RZU6	Col 21 A1	1189.8	209.1	1043.0	211.9	1288.6	422.0	n/s	n/s	n/s
F1RYI8	Col 3 A1	4462.9	911.0	4552.4	621.3	6146.3	1711.3	n/s	n/s	<0.01
I3LS72	Col 6 A1	8741.7	1350.8	9572.7	1265.6	8814.4	1224.5	n/s	n/s	n/s
Q1T7A8	Col 6 A1	1903.1	461.2	3325.3	246.1	2623.1	602.5	<0.0001	<0.01	<0.01
Q1T7A9	Col 6 A1	4092.8	740.6	6606.2	1046.6	5773.3	860.3	n/s	n/s	n/s
I3LQ84	Col 6 A2	26275.6	4568.9	33652.1	4812.7	29312.9	4881.8	n/s	n/s	n/s
Q1T7A4	Col 6 A3	6906.2	1356.2	10895.4	2267.4	9463.6	1165.9	n/s	n/s	n/s
Q1T7A5	Col 6 A3	15785.6	3517.3	24473.7	932.4	20734.4	3254.1	n/s	n/s	n/s
F1SQ10	Decorin	36435.2	7098.8	20054.4	2431.5	11143.4	690.2	<0.0001	<0.0001	<0.0001
F1RPV5	Dermatopontin	1583.7	288.1	1180.3	147.1	779.7	198.2	<0.001	<0.0001	<0.001
F1SD87	Fibulin 5 Precursor	1002.1	184.7	610.7	117.5	431.3	184.2	<0.0001	<0.0001	<0.01

F1SKM9	Galectin	1980.5	143.8	31.0	5.0	3.8	0.9	<0.0001	<0.0001	<0.0001
F1SQ09	Lumikan Keratan Sulfate Proteoglycan	20751.7	2108.5	1809.7	149.5	1297.1	383.8	<0.0001	<0.0001	<0.01
F1S6B4	Prolargin	17213.9	6219.9	1345.0	163.4	927.7	104.0	<0.0001	<0.0001	<0.0001
F1SMI5	Tenascin	13245.4	2673.1	5557.9	2265.8	9464.1	967.8	<0.0001	<0.0001	<0.0001